

## MORE ABOUT CLUSTERING ON A SCALE OF $0.1 c$

R. BRENT TULLY

Institute for Astronomy, University of Hawaii  
 Received 1987 January 21; accepted 1987 May 27

### ABSTRACT

A previous suggestion is substantiated that our Galaxy is appended to what is now called the Pisces-Cetus Supercluster Complex. This complex involves  $\sim 60$  rich clusters and  $\sim 10^{18} M_{\odot}$  and has a long dimension of  $300 h_{75}^{-1} \text{ Mpc} \approx 0.09 c \text{ km s}^{-1}$ . The evidence is twofold. (i) With a sample of rich clusters that is complete to beyond the mean distance of the complex, there is percolation across  $\sim 300 h_{75}^{-1} \text{ Mpc}$  at a separations scale length of  $38 h_{75}^{-1} \text{ Mpc}$ , a value small compared with  $\rho^{-1/3} = 54 h_{75}^{-1} \text{ Mpc}$ . The percolated structure is contained within a volume with a very low filling factor ( $\sim 0.5\%$  of the volume available) and a very high overdensity ( $\sim 25\bar{\rho}$ ). (ii) A one-dimensional correlation analysis confirms that rich clusters within the complex lie preferentially in a plane (or possibly in strata) parallel to the plane of the Local Supercluster as defined by nearby galaxies. The main plane of the Pisces-Cetus Supercluster Complex, centered  $\sim 200 h_{75}^{-1} \text{ Mpc}$  away, is coincident with the principal plane of the Local Supercluster, both in terms of the alignment of polar axes and in terms of the alignment of equatorial disks. The thickness of the Pisces-Cetus main plane has FWHM  $\sim 40 h_{75}^{-1} \text{ Mpc}$ .

The coincidence of the two planes of structure on such radically different scales suggests there is a physical connection. It would follow that the structure on a scale of  $0.1 c$  has a physical significance.

*Subject headings:* cosmology — galaxies: clustering

### I. INTRODUCTION

In a recent article (Tully 1986; hereafter T86), evidence was provided that the Galaxy is embedded in a region roughly  $30,000 \text{ km s}^{-1}$  across that is overdense in rich clusters. This apparent very large scale feature is flattened toward a plane coincident with the plane of the Local Supercluster, defined by the distribution of galaxies with  $V < 3000 \text{ km s}^{-1}$ . The overdense region would contain  $\sim 10^{18} M_{\odot}$ .

Such structure is not anticipated by most popular theories of galaxy formation. The results presented in T86 were provocative, but they were based on poor statistics and could have been biased by the nature of the sample then available. The present study provides a reasonably strong confirmation of the main conclusions in T86. The sample has been considerably enlarged, and no obvious selection effect can account for the observed pattern.

The organization of the paper is as follows. In the next section, an attempt is made to display what I think I see. In the subsequent section, characteristics of the sample are explored. It is necessary to evaluate if any selection or statistical effects could create the illusion of the purported structure. Following that, there is a more quantitative evaluation of the properties of the structure. Results of a percolation analysis and of a one-dimensional correlation analysis are discussed.

### II. MAPS

It is becoming generally appreciated that there is intricate structure in the distribution of galaxies. This belated revelation has come with growing knowledge of the three-dimensional distribution of galaxies and of clusters of galaxies as major redshift surveys have reached fruition.

Filamentary structure is not apparent in two-dimensional views because of projection confusion. Filling factors for the structure are such that lines of sight that are more than a small multiple of the dimensions of a feature will be confused. Structures

have filling factors small enough to be physically interesting but large enough to provide good camouflage. One way around this problem is to separate out what can be called the "structural components." These components can be scrutinized free of contamination by projections and then pieced together.

Figure 1 provides a very crude overview.<sup>1</sup> Guided by a percolation analysis to be described later, I conclude that there are five vast "supercluster complexes" (or "SCC") delineated by the distribution of Abell clusters with  $z < 0.1 c$ . I call these five structures the Ursa Major, Hercules-Corona Borealis, Leo, Aquarius, and Pisces-Cetus supercluster complexes. An SCC can contain of order 50 rich clusters and several 100 Mpc scale superclusters of the sort defined by Batuski and Burns (1985a) and Bahcall and Soneira (1984).

Sixty-four percent of the 315 Abell clusters with measured  $z < 0.1 c$  lie within the confines of these five features. If the features are approximated by triaxial spheroids with dimensions defined by the rms excursions from their centers of mass, the  $1 \sigma$  surfaces contain 0.4% of the available volume (which is  $\sim \frac{2}{3}$  of the total volume within  $z = 0.1 c$  since  $\sim \frac{1}{2}$  the volume is obscured and a further  $\frac{1}{3}$  is south of the Abell catalog limit). The density of Abell clusters inside the  $1 \sigma$  surfaces is 25 times the mean density.

The Aquarius SCC and the three SCCs in the north galactic hemisphere can be followed to redshifts larger than  $0.1 c$ . In the case of Ursa Major, the main part of this feature appears to be at  $0.10 < z < 0.15 c$  (Henry and Huchra 1987). There is still only sparse information about the sky below the Abell survey

<sup>1</sup> These and most other maps are plotted in Cartesian supergalactic coordinates. The Local Supercluster lies in the SGX-SGY equatorial plane. The supergalactic and galactic planes are close to orthogonal, with the SGX-SGZ equatorial plane tilted only  $6^\circ$  from the disk of the Galaxy. Proper distances,  $D_p$ , follow from redshifts,  $z$ , assuming  $H_0 = 75 h_{75} \text{ km s}^{-1} \text{ Mpc}^{-1}$  and  $q_0 = \frac{1}{2}$ :  $D_p = 4000(z - 0.75z^2)/(1 + z)$  in Mpc.

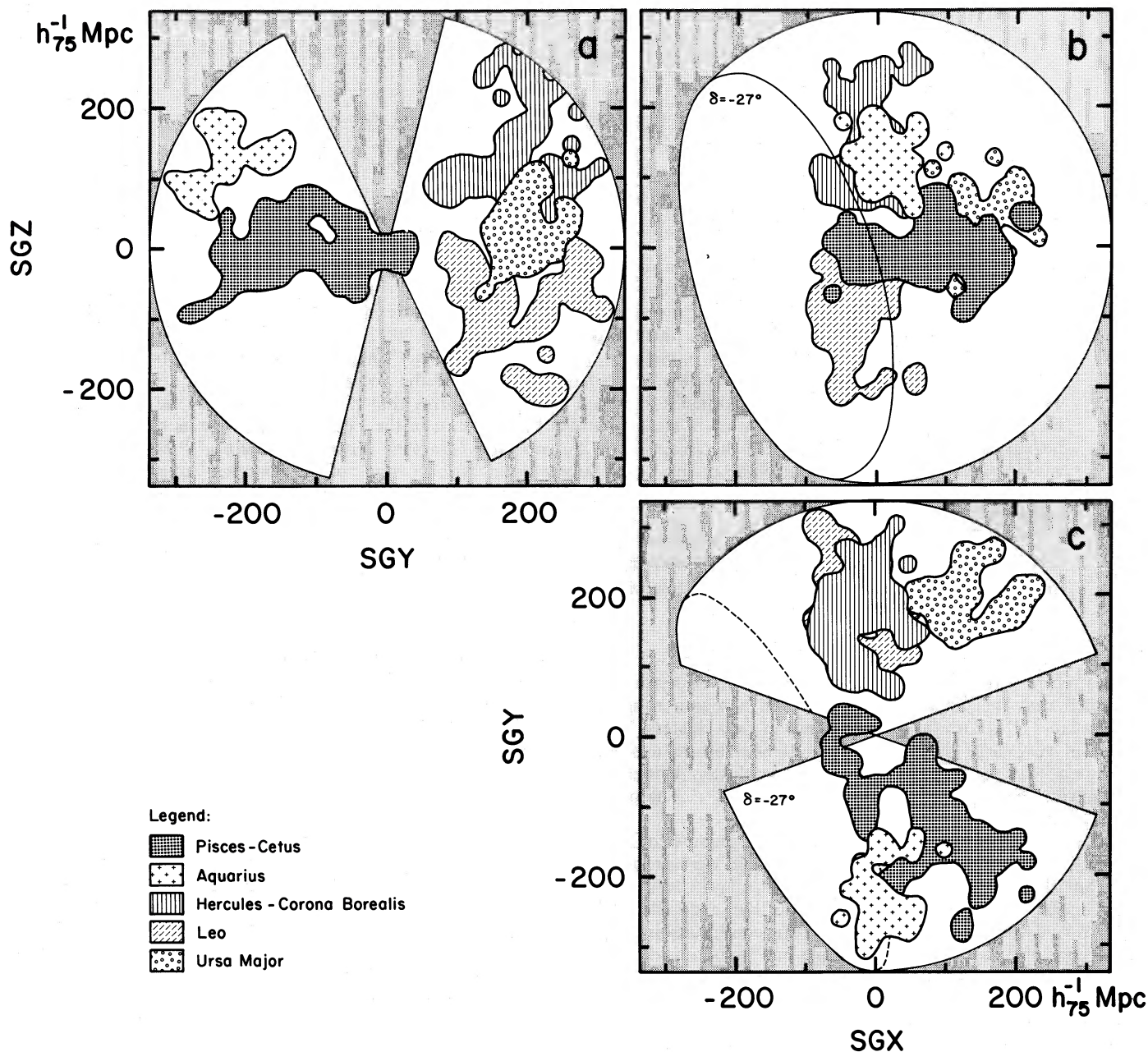


FIG. 1.—Orthogonal views of the five major supercluster complexes within  $0.1 c \approx 340 h_{75}^{-1} \text{ Mpc}$ . The supergalactic coordinate system is defined such that the Local Supercluster lies in a plane with  $SGZ = 0$ . The zone of obscuration lies about a plane  $6^\circ$  from an  $SGX$ - $SGZ$  surface at  $SGY = 0$ . The cone of incompleteness below  $\delta = -27^\circ$  primarily occupies the quadrant with  $SGX < 0$ ,  $SGY < 0$ . The intersection of this cone with the  $z = 0.1 c$  surface is shown. The three views are from (a)  $SGX = +\infty$ , (b)  $SGY = -\infty$ , and (c)  $SGZ = +\infty$ . The projected surface density contours corresponding to  $0.07 h_{75}^{-2} \text{ clusters Mpc}^{-2}$  are shown for each of the five complexes. These contours enclose 64% of the Abell clusters within  $0.1 c$ . For clarity, the distribution of the remaining clusters is not mapped.

limit of  $\delta = -27^\circ$ , but it is evident that there is a major complex in Indus at  $z \sim 0.06 c$  (Corwin and Emerson 1982).

The discussion will now focus on the region of the Pisces-Cetus SCC. In T86, it was suggested that we are associated with this specific complex. Still guided by the percolation analysis, the region is separated into what I perceive to be the structural components in the three orthogonal views of Figure 2.

The southern limit of the Abell survey of rich clusters at  $\delta = -27^\circ$  is a surface roughly through the middle of the southern galactic polar cap. The Pisces-Cetus feature can be followed to this survey limit and must be presumed to continue to more southerly locations. There is an interest in the

southern sky because we are probably part of a “Virgo-Hydra-Centaurus Supercluster” (T86) and because our most important links with the Pisces-Cetus complex could well be in the south (there are no strong local connections in the unobscured part of the northern sky). To evaluate this possibility, the sample of Abell clusters north of  $\delta = -27^\circ$  has been supplemented by whatever information is available regarding more southerly rich clusters.

In order to include the Virgo-Hydra-Centaurus region that is suspected to be associated with the Pisces-Cetus complex, the maps in Figure 2 have been carried across the zone of obscuration to a limit of  $SGY = 50 h_{75}^{-1} \text{ Mpc}$  in the northern polar cap.

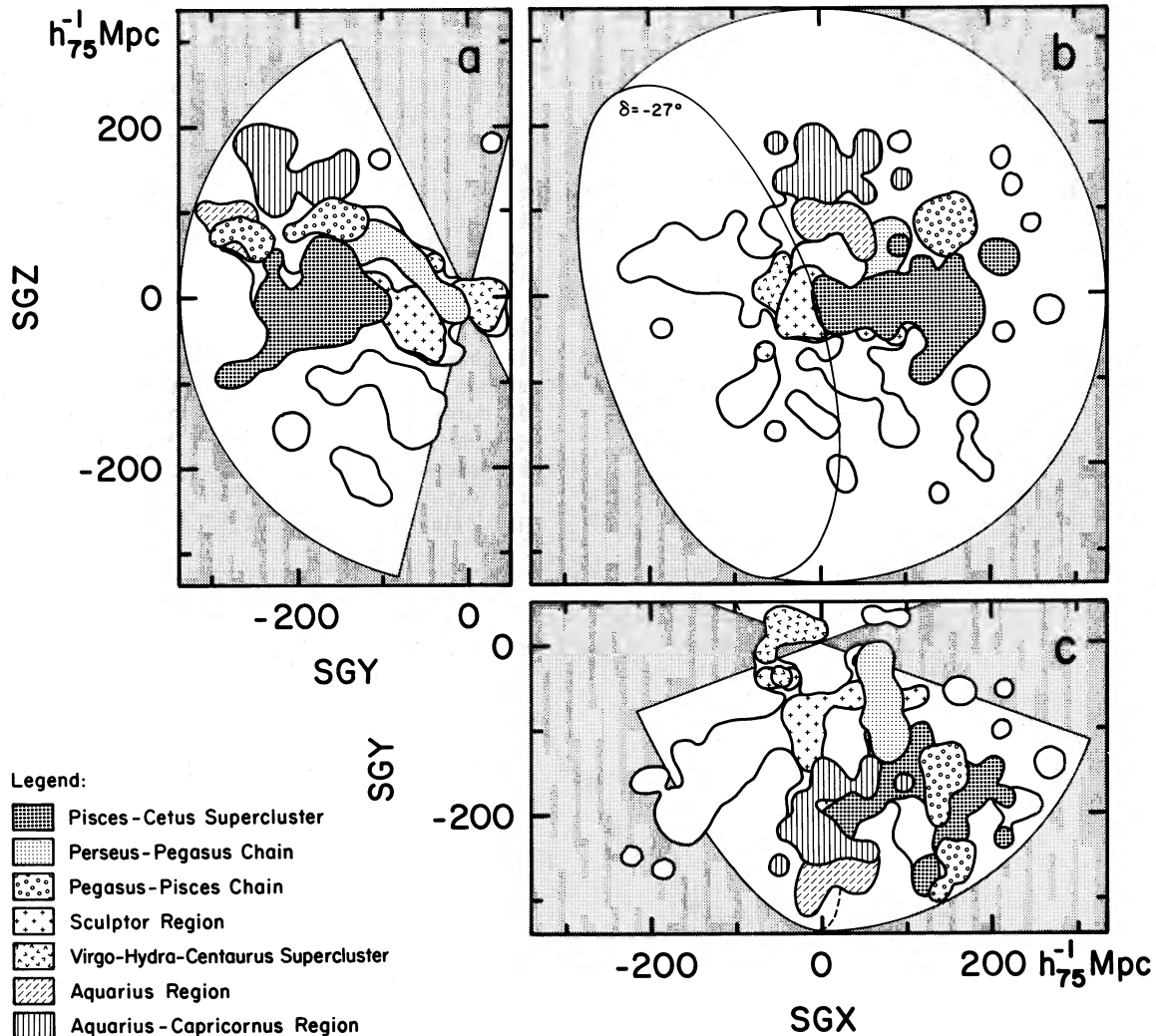


FIG. 2.—Orthogonal views of the two supercluster complexes in the south galactic hemisphere: Pisces-Cetus and Aquarius. The viewing directions, scale and contour level are the same as in Fig. 1, and the obscuration and southern incompleteness surfaces are the same. The Pisces-Cetus SCC is subdivided into five principal components, and the Aquarius SCC is subdivided into two. Clusters outside of the two main complexes lie within the unshaded regions. In each view, clusters well to the foreground or background of the two main complexes have been ignored. The substantial feature at  $SGX \sim -150$ ,  $SGY \sim -150$ ,  $SGZ \sim +30 h_{75}^{-1}$  Mpc is the incompletely surveyed Indus Supercluster.

By a percolation scale length characteristic of the sample of  $(\text{density})^{-1/3} = 54 h_{75}^{-1}$  Mpc, 75% of the 114 Abell clusters south of the galactic plane with  $z < 0.1 c$  are associated with only two supercluster complexes: the Pisces-Cetus SCC (61 clusters) and the Aquarius SCC (25 clusters). These units are subdivided into major subcomponents in Figure 2. The Aquarius SCC is separated into two parts, and a major fraction of the complex is probably beyond  $z = 0.1 c$ . The Pisces-Cetus Supercluster Complex is separated into five parts: (i) the Pisces-Cetus Supercluster, (ii) the Perseus-Pegasus chain, (iii) the Pegasus-Pisces chain, (iv) the Sculptor region, and (v) the Virgo-Hydra-Centaurus Supercluster.

The Pisces-Cetus Supercluster is the most prominent component of the complex. It has been discussed by Batuski and Burns (1985a) and in T86. This supercluster may extend below the  $\delta = -27^\circ$  limit of the Abell survey.

The Perseus-Pegasus chain and the Pegasus-Pisces chain together constitute the remarkably long filament discovered by Batuski and Burns (1985b). I describe this feature in terms of two components because there is a substantial gap and kink that is not bridged in the percolation analysis until almost the

characteristic scale length of the sample of  $54 h_{75}^{-1}$  Mpc. Nevertheless, the Batuski-Burns feature deserves serious attention. The part called the Pegasus-Pisces chain percolated into additional structure at  $z > 0.1 c$ .

The Sculptor region remains too poorly delineated to warrant the appellation “supercluster” because most of it is below the  $\delta = -27^\circ$  limit of the Abell sample. It is possible that there is a direct connection between this region and the extensive clustering in Indus (Corwin and Emerson 1982). The Virgo-Hydra-Centaurus Supercluster is also poorly defined because so much of it lies in the southern sky and in the zone of galactic obscuration.

The Virgo-Hydra-Centaurus Supercluster contains only one Abell cluster near the zone of obscuration, and its connection to the Pisces-Cetus complex cannot be argued on the basis of the percolation analysis. Rather, the association is made based on the coincidence between the plane defined by the distribution of nearby galaxies and the plane of flattening of the Pisces-Cetus SCC. This point will be discussed further.

The qualitative description provided in this section is intended to provide a general orientation. There are no other

important features in the distribution of Abell clusters in the region under consideration. If the Pisces-Cetus and Aquarius supercluster complexes are enclosed by spheroidal shells defined by the  $1\sigma$  axial excursions of clusters from each barycenter, these two shells together enclose 0.6% of the volume available with  $z < 0.1c$ ,  $\delta > -27^\circ$ , and  $b < -30^\circ$ . The density of clusters within the  $1\sigma$  surfaces is 25 times the mean density. Only 28 of 114 southern Abell clusters are *not* associated with these two complexes and no other association has more than four members.

There is a tabulation of the members of the principal supercluster complexes and cross-references with other supercluster assignments in the Appendix. There will be more maps of the sort shown in this section included in the *Nearby Galaxies Atlas* (Tully and Fisher 1987).

### III. HOW COMPLETE IS THE SAMPLE?

Actually, there are two samples. There are 315 Abell clusters with measured  $z < 0.1c$ , and there is a supplement of 67

known rich clusters within the same redshift limit but either below the Abell search limit of  $\delta = -27^\circ$ , or with velocity dispersions greater than  $600 \text{ km s}^{-1}$ , or otherwise judged to be rich enough to have been included in the Abell catalog. The properties of the supplemental sample are very poorly understood. It only serves to provide us with a qualitative glimpse of the southern sky where many of the nearest clusters seem to be and, also, as a check on completion aspects of the Abell catalog. The remaining discussion in this section will deal with just the better defined Abell sample of 315 clusters.

All but 26 of 251 Abell clusters with distance class  $\leq 4$  now have publicly disseminated velocities (Struble and Rood 1987; Huchra and Postman 1986), and the few clusters in these classes with undetermined velocities are spread across the sky. By contrast, only 490 of 2461 Abell clusters with distant class  $\geq 5$  have known velocities, and the sky coverage is very inhomogeneous. There are three particularly well sampled parts of the sky (Ciardullo *et al.* 1983; Ciardullo, Ford, and Harms 1985; Henry and Huchra 1987). However, in each of the deeply

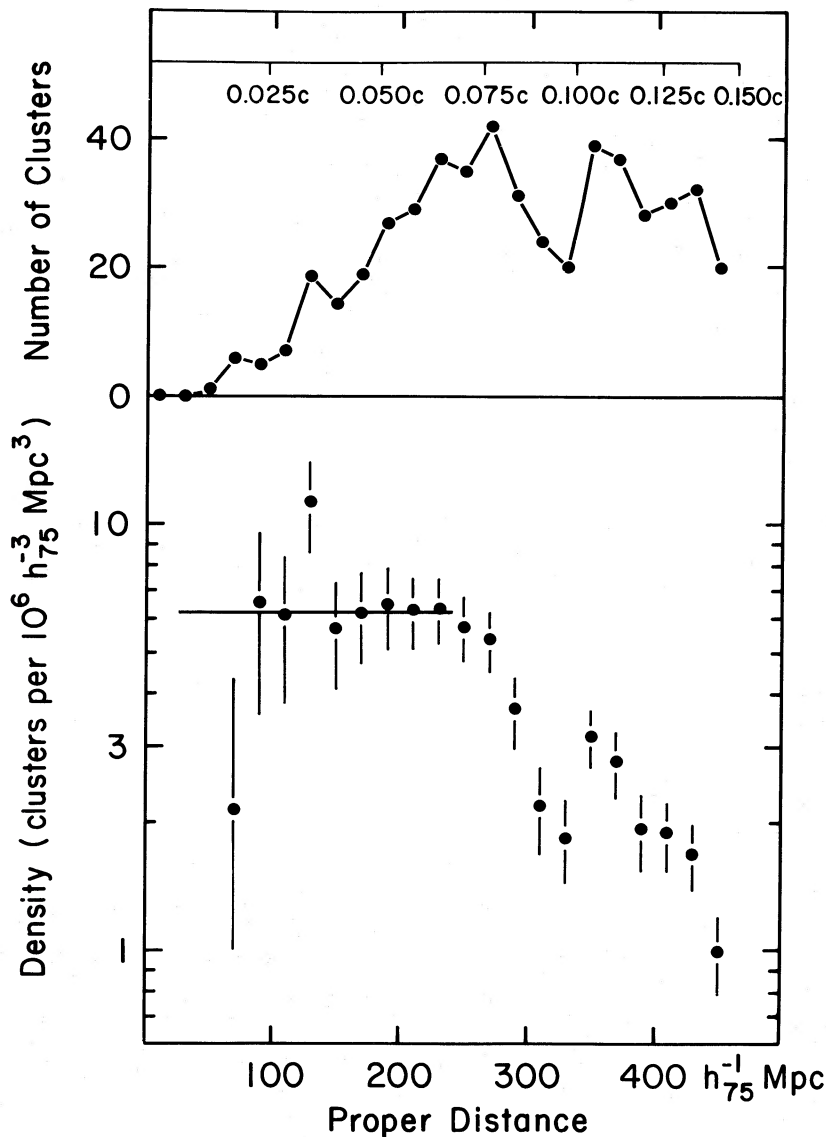


FIG. 3.—*Top panel*: number of Abell clusters with known redshift per  $20 h_{75}^{-1} \text{ Mpc}$  interval of distance. The correspondence between distance and redshift is shown. *Bottom panel*: density of Abell clusters with known redshift as a function of distance. The error bars indicate  $N^{1/2}$  uncertainties. The region of completion is within  $240 h_{75}^{-1} \text{ Mpc}$ , and the mean density in this region is indicated by the horizontal line.

sampled regions, the great majority of the distance class  $\geq 5$  clusters are at  $z > 0.1 c$ . The biases introduced by abnormal completion in these regions is small for  $z < 0.1 c$ .

Figures 3 and 4 provide details of the present coverage. The number of clusters with observed redshifts per distance interval is shown in the top panel of Figure 3, and the corresponding run of density with distance is shown in the bottom panel of Figure 3. Figure 4 illustrates the percentage of clusters with observed redshifts  $z < 0.1 c$  as a function of  $m_{10}$ , the apparent magnitude of the tenth brightest cluster member. If  $m_{10} \leq 16.7$ , the percentage with  $z < 0.1 c$  is greater than or equal to 50%. The curve in this figure shifts with redshift limit in the expected fashion (i.e., for  $z < 0.05 c$  the 50% point shifts to  $m_{10} \approx 15.2$ ).

Apparently, there is good completion at present to 20,000  $\text{km s}^{-1} \approx 240 h_{75}^{-1}$  Mpc, with rapidly diminishing completion at greater distances. The expected incompleteness as a function of redshift can be calculated, given the model for incompleteness as a function of  $m_{10}$  provided by Figure 4 and knowledge of the number of clusters without observed redshifts as a function of  $m_{10}$ . The conclusion is that incompleteness in the Abell sample begins at  $z \approx 0.06 c$ , that there is 70% completion within  $z = 0.075 c$ , and 50% completion within  $z = 0.1 c$ .

There may be concern that apparent structure could be an artifact either because Abell clusters have been unevenly sampled in the process of the velocity measurements or because Abell did not evenly survey the sky originally. Figures 5 and 6 are plotted in an attempt to allay that concern. Figure 5 is a display of the 315 Abell clusters with observed redshifts  $z < 0.1 c$ . Figure 6 is a display of 853 Abell clusters *without* observed redshifts and distance class  $\leq 5$ . Roughly 30% of the clusters plotted in Figure 6 are expected to have  $z < 0.1 c$ .

There is the obvious deficiency of clusters without known velocities in Figure 6 at  $l \sim 125$ ,  $b \sim 50$ , the consequence of the deep survey by Henry and Huchra (1987). However, there is

not a marked overdensity at the corresponding location in Figure 5 (as there would have been if the plot were extended to a deeper redshift limit).

The supercluster complexes are not particularly evident in these figures. Both the sampling of the unobscured part of the sky by Abell and the sampling of the catalog by redshift observers seems reasonably random. It is difficult to see how the *extreme* clustering, with filling factors less than 1%, could be an artifact of the observations.

#### IV. A PERCOLATION ANALYSIS

The point of the present section is to show that percolation occurs across vast dimensions with a very low value of the percolation scale length parameter. Einasto *et al.* (1984) have discussed the use of percolation analysis in the context of galaxies in the vicinity of the traditional Local Supercluster. Batuski and Burns (1985a) and Batuski, Melott, and Burns (1987) have done a similar study with Abell clusters. In each of these cases, simulations were also analyzed.

In a percolation analysis, if any two units are closer together than a specified scale length, then they are linked together. This prescription can lead to a network of such linkages. The procedure is particularly appropriate for the delineation of filamentary structures, where the mean density in a spherical domain might still be low.

The percolation scale length can be compared with a scale length characterized by the mean density of the sample. From Figure 3, the mean density in the region of completion is determined to be  $\bar{\rho} = 6.2 \times 10^{-6} h_{75}^3$  clusters  $\text{Mpc}^{-3}$ , whence the mean density characteristic scale length is  $R_a = \bar{\rho}^{-1/3} = 54 h_{75}^{-1}$  Mpc. Einasto *et al.* (1984) introduced the scale length  $R_0 = (3/4\pi)^{1/3} R_a = 34 h_{75}^{-1}$  Mpc and the percolation parameter  $B(r) = (R/R_0)^3 = r^3$ .

The critical percolation scale length,  $R_p$ , is defined as the

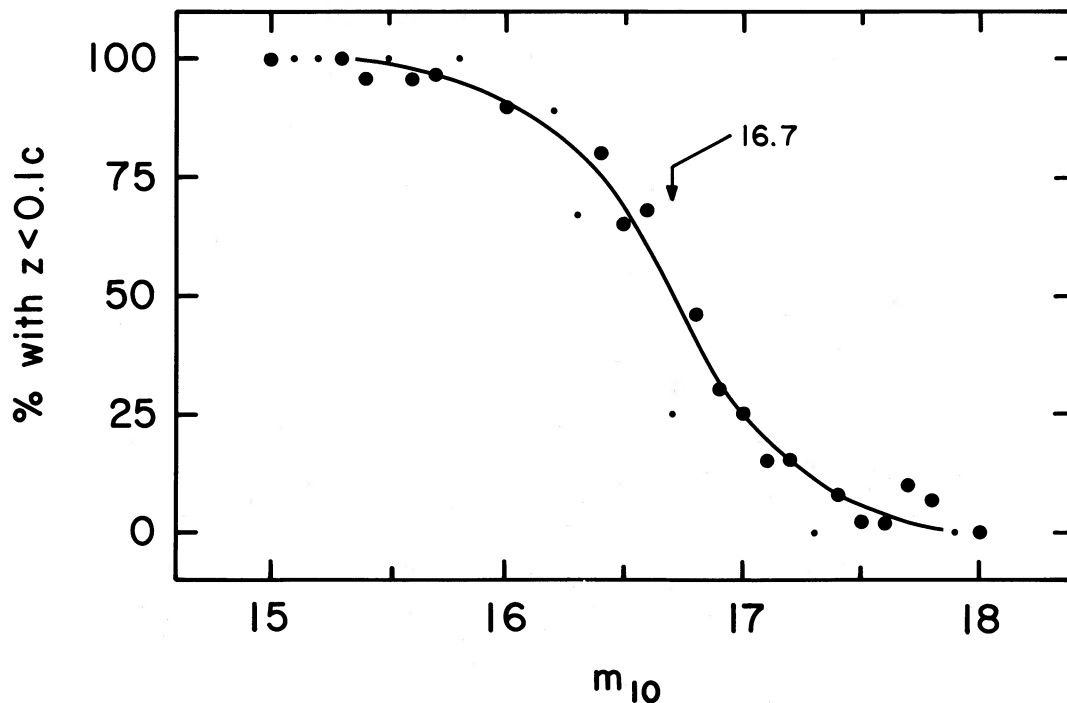


FIG. 4.—Percentage of Abell clusters with measured redshifts that are less than  $0.1 c$  as a function of  $m_{10}$ , the magnitude of the tenth brightest galaxy in a cluster. The curve drops to 50% at  $m_{10} = 16.7$  mag.

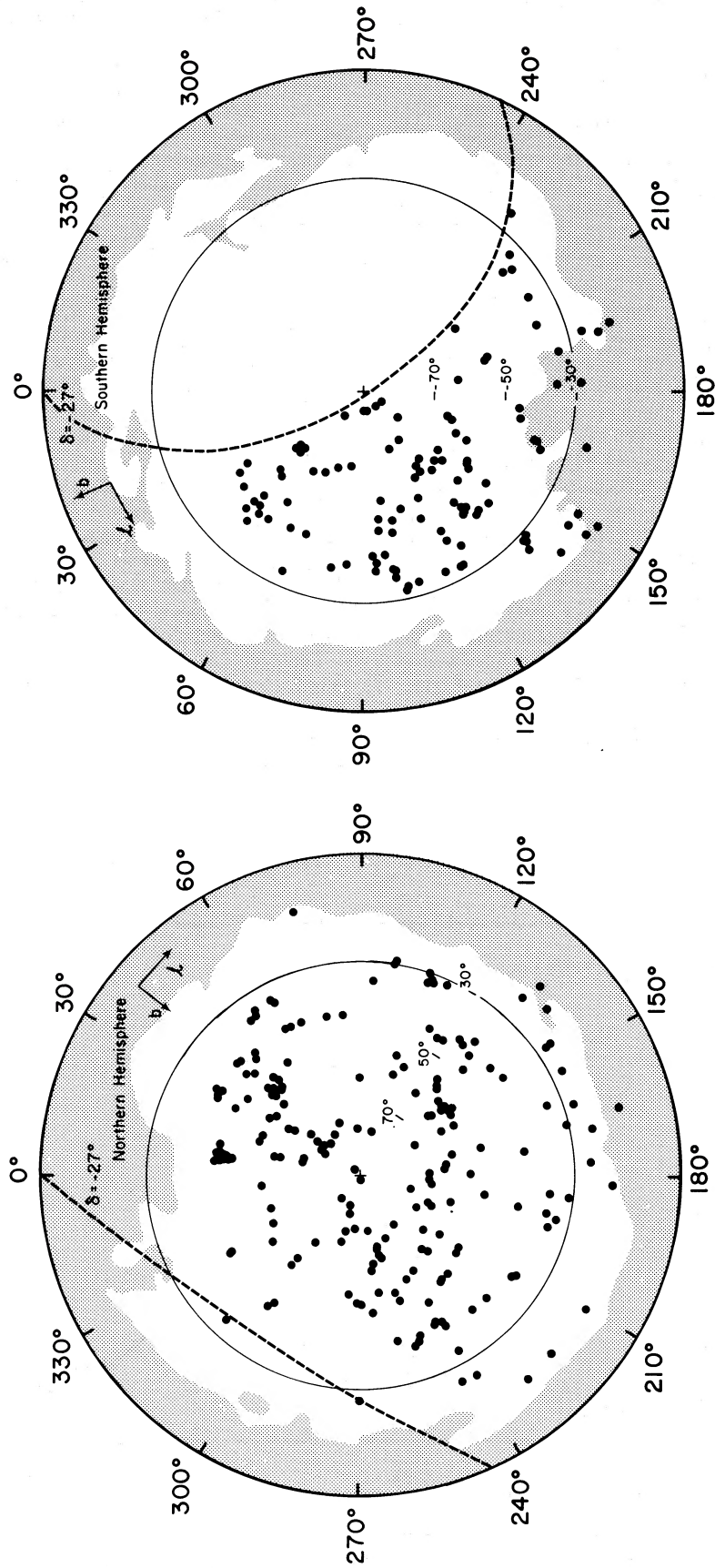


FIG. 5.—Distribution of Abell clusters with measured redshifts less than 0.1  $c$ , in galactic coordinates. *Left panel:* northern hemisphere. *Right panel:* southern hemisphere. The  $\delta = -27^\circ$  limit and  $|b| = 30^\circ$  circles are indicated. The outer shaded areas lie outside the Burstein-Heiles HI contour that corresponds to  $A_B = 0.5$  mag.

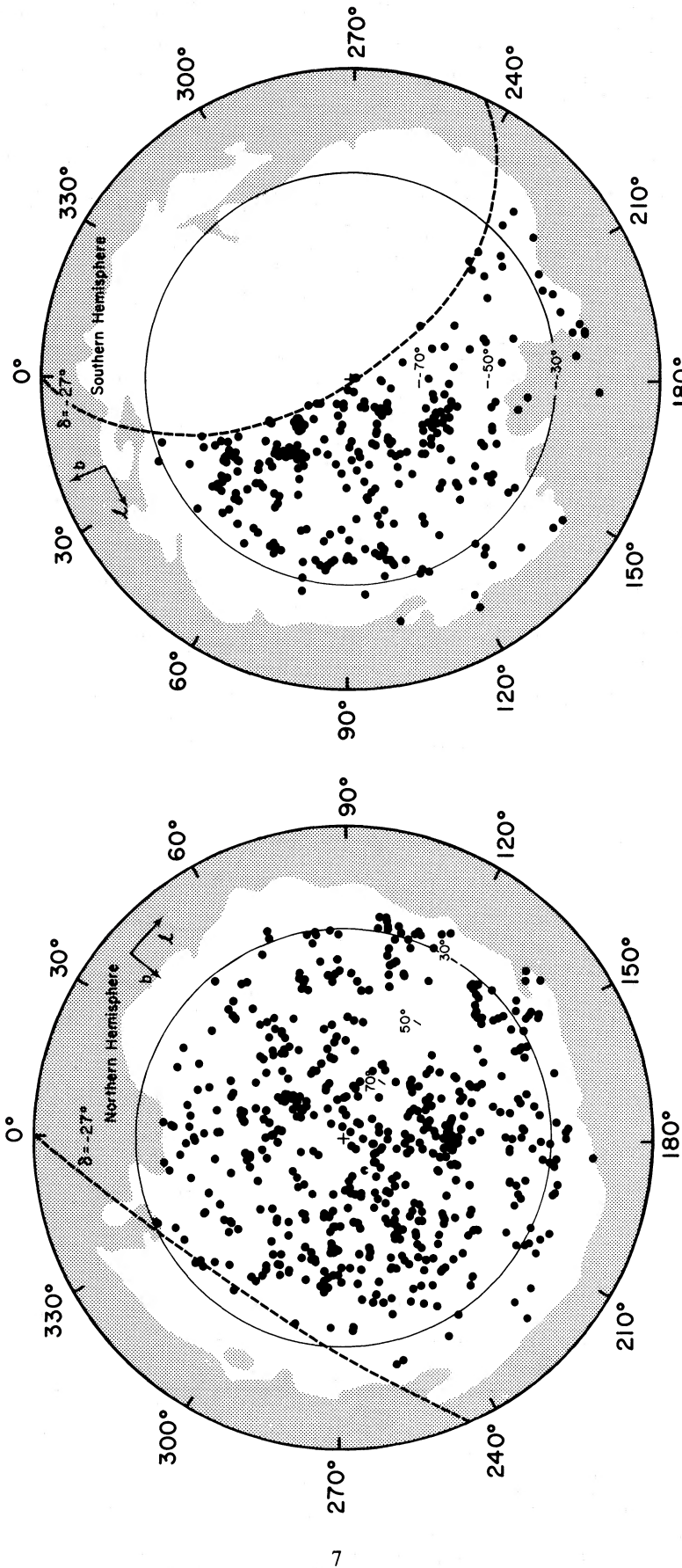


FIG. 6.—Distribution of Abell clusters without measured redshifts but with distance class  $\leq 5$ . Otherwise, similar to Fig. 5.

scale length that causes percolation to propagate across the dimensions of the sample. The boundaries are soft with our observed sample. There is incompleteness at large radial distances and because of the intersection of the sample with the zone of obscuration. Due to the latter problem, the north and south galactic hemispheres will be considered separately. The resultant volumes are shaped like ice cream cones with wide opening angles. The southern cone is cut in half by the declination limit, while the northern cone is almost complete. The axial extent of the cones are  $0.1 c = 340 h_{75}^{-1}$  Mpc (if  $q_0 = \frac{1}{2}$ ), with incompleteness significant beyond  $240 h_{75}^{-1}$  Mpc. Given the unusual shapes and soft boundaries of the volumes, it is sufficient to describe them by a "characteristic dimension" for traversal,  $D_c$ , with  $D_c \approx 300 h_{75}^{-1}$  Mpc. We ask at what value of  $R_p$  is there percolation across distances of order  $D_c$ .

The dimensions associated with percolated structure are described by the three-dimensional diagonal of the smallest box that accommodates all the members of a unit. The largest dimensions of percolated structures in each hemisphere are plotted in Figure 7 as a function of the choice of percolation scale length. The maximum percolation dimension in each volume reaches the characteristic size  $D_c$  with  $R_p = 38 h_{75}^{-1}$  Mpc. The corresponding value of the percolation parameter is  $B_p = 1.4$ . Couched closer to the terminology of Batuski, Melott, and Burns (1987),  $R_p/R_a = 0.70$ .

As the percolation scale is increased beyond  $R_p$ , the maximum percolation dimension plateaus and then, at  $R \sim R_a$ , increases to the largest possible values commensurate with the volume under study. By this sort of scale, the various supercluster complexes are linking. Each of these entities separately has dimensions of order  $D_c$ . The structures are so large that it

is not possible to distinguish between two obvious alternatives: (a) that the supercluster complexes are distinctive entities, or (b) that they would link together with  $R \sim R_p$  if a large enough volume could be surveyed.

There are no simulations of structure on sufficiently large scales to compare with the above result. It seems evident from the Einasto *et al.* (1984) work, though, that  $B_p = 1.4$  is a very low value for the percolation parameter. It favors the increasingly popular notion that a network of connected filaments exists.

#### V. THE FLATTENED LOCAL SUPERCLUSTER COMPLEX

We are now getting into what I consider to be the most fundamental issue raised in this paper. Much of the motivation for the claim in T86 that we are appended to a vast supercluster complex came from the observation that relatively nearby rich clusters (those within  $100 h_{75}^{-1}$  Mpc) adhere to the same plane as that defined by the distribution of nearby galaxies (those within  $40 h_{75}^{-1}$  Mpc) and, moreover, rich clusters in the Pisces-Cetus Supercluster (at a distance of  $\sim 200 h_{75}^{-1}$  Mpc) adhere remarkably to the very same plane.

Figure 8 is offered by way of introduction to this discussion. It is a plot of number of clusters as a function of distance from the plane defined by the distribution of nearby galaxies. It is based on a sample of 358 clusters with observed redshifts less than  $0.1 c$ : the sample of Abell clusters and supplementary rich clusters used in the construction of the maps in § II, except that clusters associated with the incompletely surveyed Indus complex in the south have been excluded. This diagram is an update of Figure 5 in T86. As in that earlier plot, the top panel has been normalized to account for (i) the relative volumes of

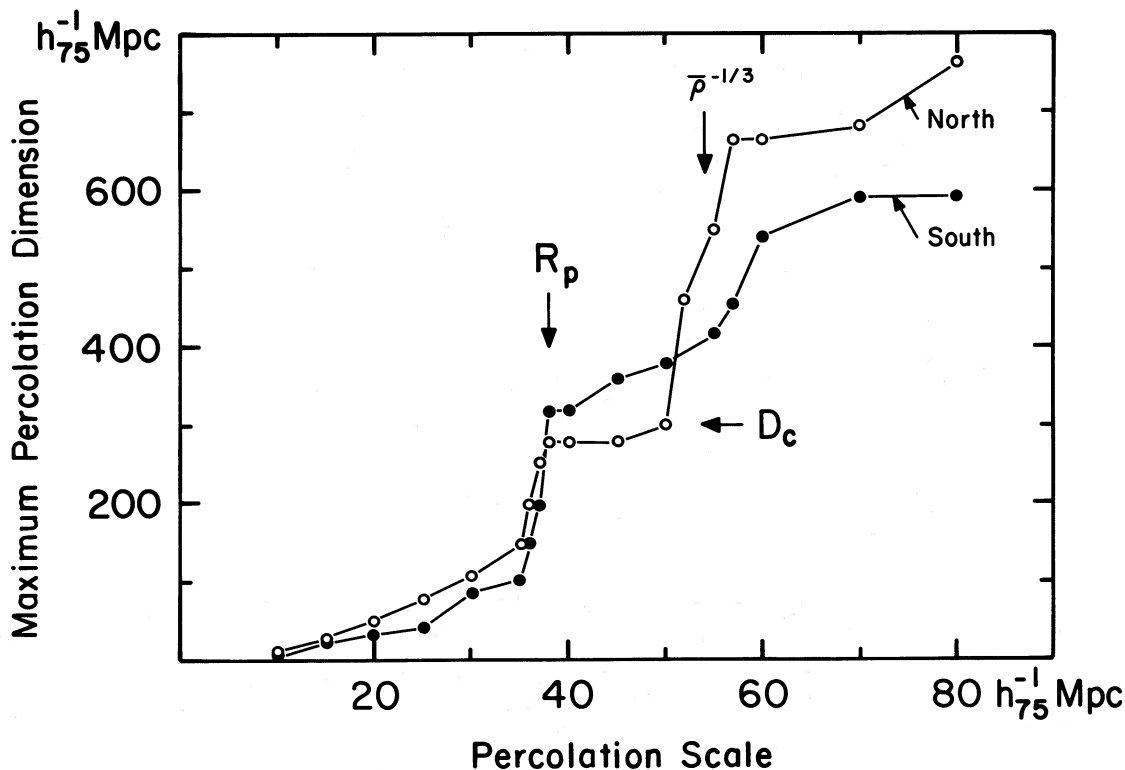


FIG. 7.—Dependence of the maximum percolation dimension on the choice of percolation scale length. North and south galactic hemispheres are plotted separately. The characteristic dimension for traversal of the volume is  $D_c = 300 h_{75}^{-1}$  Mpc. Percolation occurs across this dimension at  $R_p = 38 h_{75}^{-1}$  Mpc. The characteristic scale length defined by  $(\text{density})^{-1/3}$  is  $54 h_{75}^{-1}$  Mpc.

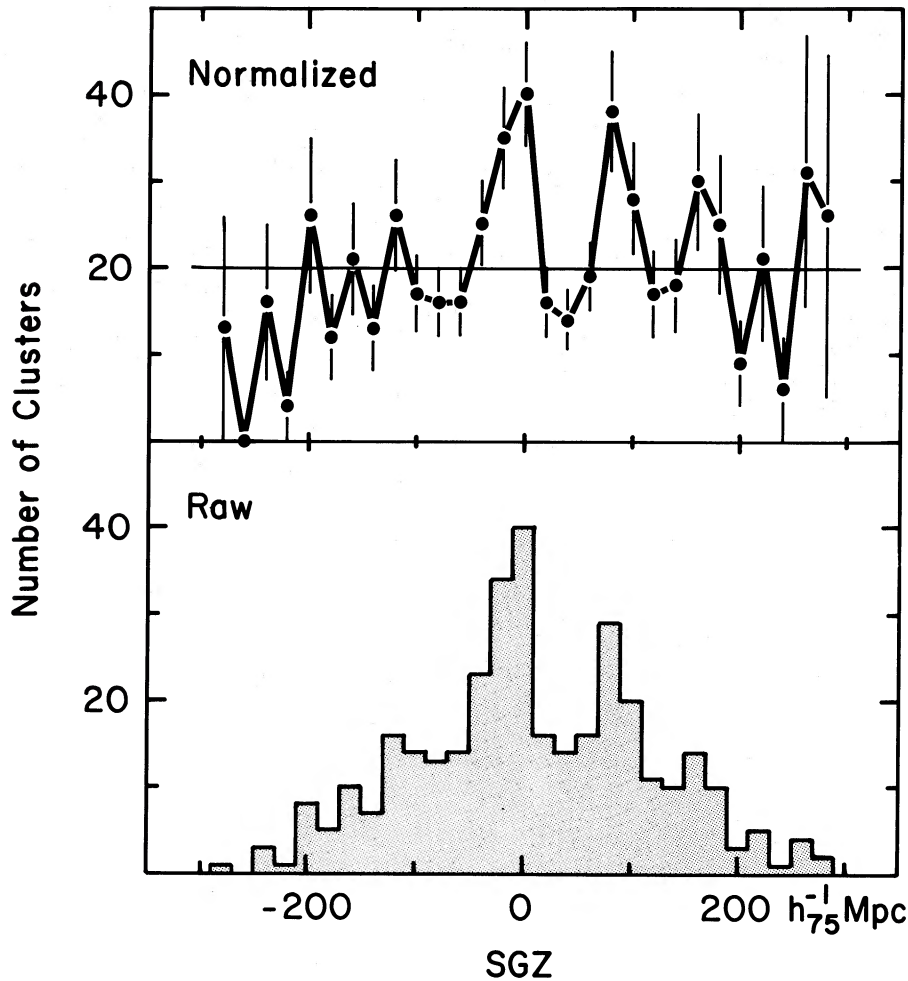


FIG. 8.—Number of rich clusters as a function of distance from the supergalactic equatorial plane. *Bottom panel*: observed numbers. *Top panel*: normalized to take into account geometric effects, obscuration, and incompleteness as a function of distance. Error bars follow from  $N^{1/2}$  statistics. The horizontal line at 20 clusters corresponds to the average count per bin after normalization.

the separate SGZ bins within the survey region, and (ii) the relative effects of obscuration on the separate SGZ bins. Moreover, the normalization now also accounts for (iii) incompleteness as a function of distance, on the assumption that all of the decrease in the density of clusters with distance is an incompleteness effect. A  $3.3 \sigma$  signal (in two bins) is seen coincident with the supergalactic equator.

The signal associated with a feature on the supergalactic equator is *stronger* with the larger and less biased sample now available than it was in T86. There is contribution to this signal from both galactic hemispheres, over wide angles. The correction factors associated with the normalization in Figure 8 are substantial but are characterized by a smooth function with  $\text{FWHM} \sim 300 h_{75}^{-1} \text{ Mpc}$ . By contrast, the signal associated with the supergalactic plane has  $\text{FWHM} \sim 40 h_{75}^{-1} \text{ Mpc}$ . These factors, combined with matters discussed in § III, lead me to conclude that the following possible explanations for the existence of the signal can be discounted: (i) galactic obscuration, (ii) incompleteness in the south celestial hemisphere, (iii) biased sampling in the acquisition of redshifts of Abell clusters, and (iv) biased sampling in the compilation of the Abell catalog.

The only tenable explanation that does not admit to the physical reality of the feature is a statistics of small numbers

hypothesis. Clusters clearly associate on scales of  $\sim 100 h_{75}^{-1} \text{ Mpc}$ , and in a volume that only includes of order 15 such elements, the chance superposition of several superclusters of this more traditional scale to give a  $3 \sigma$  signal is not improbable. This hypothesis was given support when equivalents to Figure 8 were plotted for a large number of randomly chosen axis orientations. Three sigma signals were found in a significant fraction ( $\sim 15\%$ ) of cases. These cases can be anticipated if one takes the maps in Figure 1 and asks if there are viewing angles that cause major features to project onto one another.

However, strong evidence will now be presented that the signal in Figure 8 actually is physically meaningful. This new evidence involves the equivalent of a one-dimensional correlation function. It is known that the three-dimensional function has the dependence  $\xi \sim r^{-1.8}$  (Bahcall and Soneira 1983; Postman, Geller, and Huchra 1986). If clusters were randomly oriented with respect to each other with regard to the three orthogonal axes of an arbitrary coordinate system, the correlation functions associated with one-dimensional projections are expected to be approximately flat; i.e., the number of clusters per logarithmic unit projected separation interval will be virtually independent of projected separation. If, on the other hand, clusters are preferentially confined to a sheet, then, in a projection onto an axis perpendicular to this sheet, there will

be an overabundance of small separations and a dearth of large separations and the consequence will be a steeper one-dimensional correlation function along this axis.

As a test case, it is instructive to perform the analysis on the *Nearby Galaxies Catalog* sample (Tully 1987; hereafter NBG catalog) of 2367 galaxies within  $3000 \text{ km s}^{-1}$ . As seen in Figure 1 of T86, there is overwhelmingly strong evidence of the existence of a flattened plane in that sample, and it is also claimed that there are significant secondary strata.

The results of analyses of three separate samples drawn from the NBG catalog are presented in Figure 9. Advantage is taken of the fact that the great circle of the supergalactic plane passes close to the pole of the galactic coordinate system. The SGY axis lies within  $6^\circ$  of this pole, and the SGX-SGZ plane at  $\text{SGY} = 0$  is essentially coincident, within this same angle, with the plane of the Galaxy. Consequently, all one-dimensional projections in the SGX-SGZ plane are affected in roughly equivalent

ways by the two major selection effects of obscuration and incompleteness as a function of distance. The NBG catalog provides an all-sky sample that is not significantly affected by other directional biases.

The experiment is to determine the slope of the one-dimensional frequency distribution as a function of position angle in the SGX-SGZ plane. At position angle  $0^\circ$  the frequency function along the SGX axis is formed, and at position angle  $90^\circ$  the frequency function along the SGZ axis is formed. There is no attempt to normalize as is required to derive a true correlation function because the normalization requires modeling of boundary effects and incompleteness factors. We only care if there is a *change in slope* of the frequency function in a situation where the normalization factors are uncertain but independent of position angle.

It is seen in Figure 9 that the slope at a typical position angle is  $-0.05$  for the full NBG sample of 2367 galaxies, but that

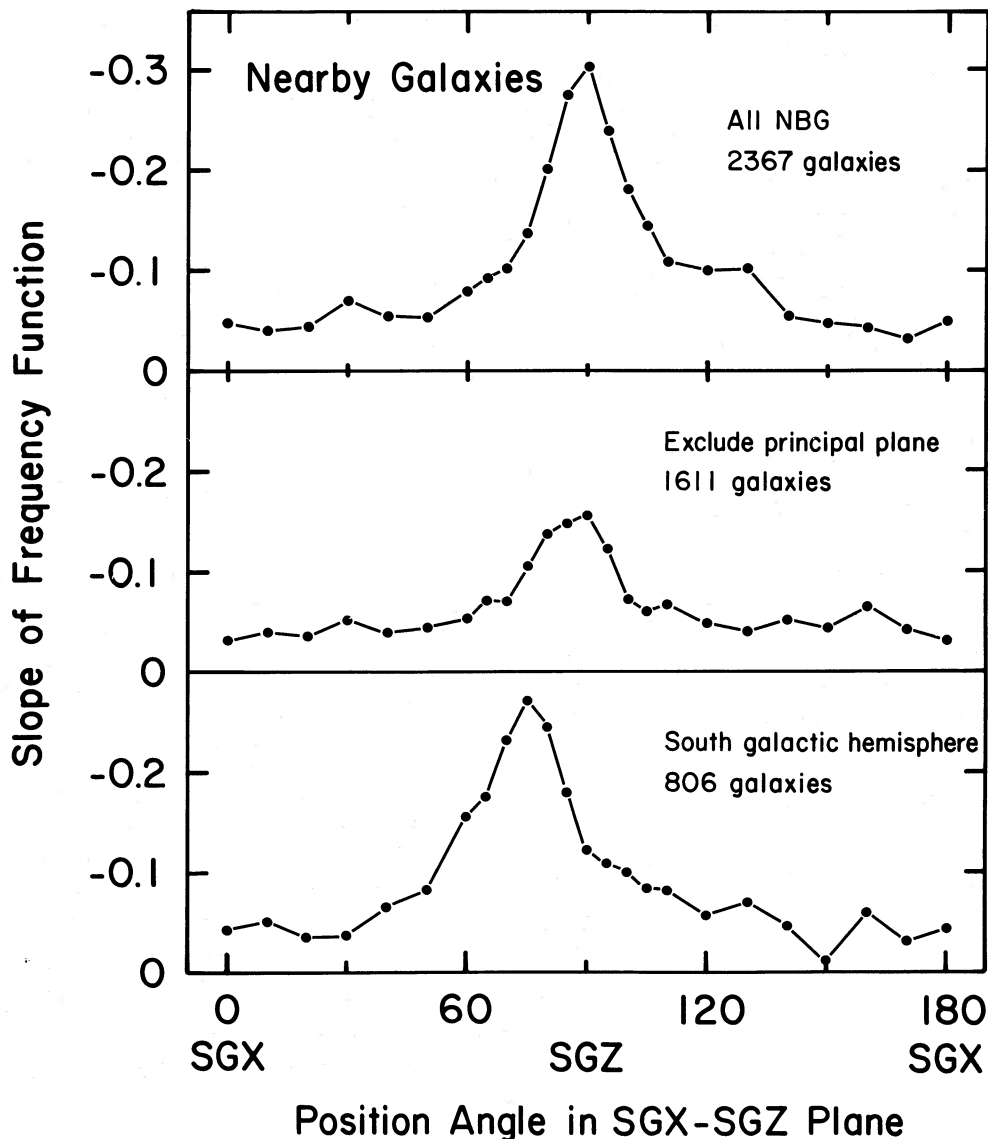


FIG. 9.—The dependence of the slope of the one-dimensional frequency function on position angle for samples of nearby galaxies. One-dimensional projections are taken at intervals in the SGX-SGZ plane. Three samples are considered. In each case, there is a significant steepening of the slope within  $15^\circ$  of the orientation associated with projections onto the SGZ axis.

there is a highly significant steepening of the frequency function to a slope of  $-0.30$  at position angle  $90^\circ$ , the angle associated with the SGZ axis.

Two subsamples confirm the claim that there is significant layering of nearby galaxies parallel to, but off, the principal plane of the Local Supercluster. A sample of 1611 galaxies is formed with all systems in the NBG catalog *except* those associated with the major constituents of the principal plane: the Virgo Cluster and Southern Extension, the Ursa Major Cluster and Cloud, the Ursa Major Southern Spur, and the Coma-Sculptor (local) Cloud. There is still a significant steepening of the frequency function slope to  $-0.16$  normal to the supergalactic equator, in this case.

Alternatively, it is instructive to consider only galaxies in the southern galactic hemisphere, since the plane of the Local Supercluster is predominantly a feature of the northern hemisphere. There are 806 galaxies in this case, and the slope of the frequency function peaks at a highly significant value of  $-0.27$ . The position angle at maximum steepening is shifted to  $75^\circ$ , but this difference of  $15^\circ$  from the SGZ axis is consistent with the layering hypothesis, with allowance for some corrugation.

Now that the effectiveness of the one-dimensional correlation analysis has been demonstrated on a local sample of galaxies, the same procedure can be applied to my sample of 358 rich clusters with  $z < 0.1 c$  (excluding the incompletely surveyed Indus region). In fact, the analysis will be performed separately on the two galactic hemispheres because the most prominent flattened structure is associated with the Pisces-Cetus complex in the south. There may be some flattened structure in the north, but the evidence is not very convincing.

In Figure 10, the slopes of the frequency distribution are plotted as a function of position angle in the SGX-SGZ plane

for the northern and southern data separately. With the 213 clusters north of the galactic plane ( $SGY > 0$ ), there is a weak but insignificant signal at position angle  $95^\circ$ . On the other hand, with the 145 clusters south of the galactic plane, there is a signal with  $3.0 \sigma$  significance peaked at position angle  $90^\circ$ ; that is, coincident with the SGZ axis. The slope of the frequency function steepens from the mean value of  $-0.04$  to a value of  $-0.15$  at the peak.

It was pointed out that SGX-SGZ surfaces are sufficiently symmetric with respect to the plane of our Galaxy that the feature is not ascribable to obscuration. The  $\delta = -27^\circ$  completion limit of the Abell catalog has almost no effect on the northern sample but would cause a *flattening* of the frequency distribution toward position angle  $90^\circ$ , which may explain the apparent broad trough that underlies the signal at  $90^\circ$ . The declination limit causes observed SGX-SGZ surfaces in the south to be roughly half-moon-shaped, with the SGX axis directed across the narrow waist and the SGZ axis directed tip-to-tip. The observational confinement in the SGX direction would tend to force correlations along that axis to be steeper. The peak in the frequency function slope along the SGZ axis occurs *in spite of* this inhibiting effect.

Just from the distribution of clusters as viewed on maps of the Pisces-Cetus region like those in Figure 2, it appears that the SGZ frequency correlations receive contributions from structure off the principal plane. That is, there may be layering of the structure, with a secondary concentration of clusters  $\sim 100 h_{75}^{-1}$  Mpc above the principal plane (also suggested by the secondary peak in Fig. 8). This layering may be analogous to the layering that can be identified with considerably more confidence in the distribution of nearby galaxies. It would be very surprising and important if it turns out to be true that

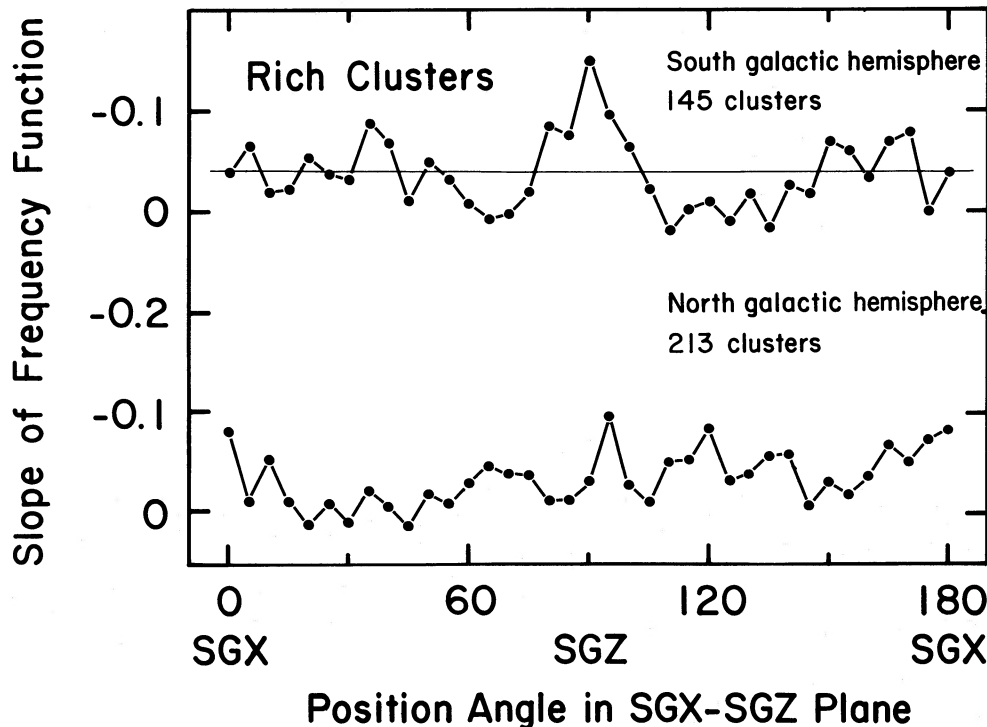


FIG. 10.—The slope of the one-dimensional frequency function as a function of position angle for samples of rich clusters. There is a  $3 \sigma$  signal aligned with the SGZ axis in the case of the southern hemisphere sample. The average slope of  $-0.04$  is indicated by the horizontal line.

there is layering on 100 Mpc scales. The present evidence in this regard is tentative.

The emphasis in this paper is on the rather strong evidence for the existence of the first-order effect: the very pronounced flattening of the general Pisces-Cetus region toward a plane coincident with the plane defined by galaxies in the local neighborhood.

#### VI. SUMMARY

In T86, tentative evidence was presented that the traditional Local Supercluster is appended to a clustering complex that is centered in Pisces-Cetus at a distance of  $16,000 \text{ km s}^{-1} \approx 200 h_{75}^{-1} \text{ Mpc}$ . This new investigation corroborates the previous work. There are two fundamental observational questions: (i) Should physical significance be attached to the largest apparent structure? (ii) Should physical significance be attached to the apparent flattening? I would argue that these questions couple, in the sense that if the answer to one is "yes," the answer to the other must be "yes" as well. Let us review the evidence.

1. The percolation analysis leads to the identification of the principal structural components, and these are found to occupy only a small fraction of the volume available ( $1 \sigma$  surfaces enclose 0.4%–0.6% of the total volume; densities within  $1 \sigma$  surfaces are  $\sim 25\bar{\rho}$ ). There appear to be five major complexes at least partially within the volume with  $z < 0.1 c$ ,  $\delta > -27^\circ$ ,  $|b| > 30^\circ$ .

2. Percolation across dimensions characteristic of the volume under study occurs at the small value of the percolation scale length of  $38 h_{75}^{-1} \text{ Mpc}$  (the value of the Einasto *et al.* percolation parameter is  $B_c = 1.4$ ). The percolation scale length is small in spite of the small filling factor.

3. The percolation analysis suggests that the relatively nearby Perseus-Pisces Supercluster is appended to the Pisces-Cetus complex. There are no obvious direct links between us and the Perseus-Pisces region, but our view is restricted by the zone of obscuration and incompleteness in the south celestial hemisphere.

4. There is evident flattening in the distribution of rich clusters in the south galactic hemisphere to the plane defined by much nearer galaxies (the principal plane of the Local Supercluster). Figure 8 suggests that this claim is true, but the most convincing evidence is provided by Figure 7 in T86,

which shows the adherence of only moderately rich Shane-Wirtanen clusters (Shectman 1985) to the same plane.

5. The densest part of this planar complex is located in Pisces-Cetus at a distance of  $200 h_{75}^{-1} \text{ Mpc}$ . The thickness of the plane is very small (FWHM  $\sim 40 h_{75}^{-1} \text{ Mpc}$  as defined by Abell clusters; FWHM  $\sim 25 h_{75}^{-1} \text{ Mpc}$  as defined by Shane-Wirtanen clusters) in contrast with the apparent length (percolation diagonal  $\sim 300 h_{75}^{-1} \text{ Mpc}$ ). Estimates of the thickness have tended to go *down* as statistics improve and smoothing is decreased, while estimates of the long dimension have tended to go *up* as completion and the survey volume are enlarged.

6. Most important, the one-dimensional correlation analysis confirms the statistical significance of the apparent flattening and the coincidence between the planes defined by rich clusters in the south galactic hemisphere and by nearby galaxies.

If it is accepted that there is a *physical* significance in the coincidence of the two planes, this must be tantamount to acceptance that our local area is associated with the Pisces-Cetus complex. The complex would contain of order 60 rich clusters that, in themselves, would incorporate  $\sim 10^{17} M_\odot$ . If 10% of galaxies are in clusters, then  $\sim 10^{18} M_\odot$  would be involved. The complex is described by a long dimension of  $300 h_{75}^{-1} \text{ Mpc}$ , a flattened plane with thickness FWHM  $\sim 40 h_{75}^{-1} \text{ Mpc}$ , filamentary structure such as the Perseus-Pegasus and Pegasus-Pisces chains (the Batuski-Burns filament) and, possibly, layering parallel to the supergalactic equator.

Within  $z = 0.1 c$  there are four other apparent supercluster complexes involving similar numbers of rich clusters and comparable dimensions. These complexes can be followed to the boundaries of the present sample. Hence, there is no reason to believe that we are yet seeing a fair sample of the universe. The complexes described here overflow the volume of space that has been surveyed, and there are no good observational limits on how large they might be.

These observations present an obvious challenge to most popular theories of galaxy formation.

Pat Henry, John Huchra, and Marc Postman generously provided unpublished redshifts for several Abell clusters.

#### APPENDIX

My delineation of five major supercluster complexes is based on a percolation analysis. The members of my current catalog of 315 Abell clusters and a total of 382 clusters with  $z < 0.1 c$  are given the complex assignments indicated in Table 1. Clusters *not* identified with the five major complexes are listed at the end of the table. The following information is provided.

Column (1): If there is an asterisk, there is percolation to the major component of one of the five major complexes by a scale length of  $40 h_{75}^{-1} \text{ Mpc}$ . If not, there is percolation by  $50 h_{75}^{-1} \text{ Mpc}$ . If there is a dagger, the cluster is part of the apparent complex in the incompletely surveyed Indus region.

Column (2): Abell name or name based on R.A. and declination.

Column (3): Adopted redshift.

Columns (4)–(6): Supergalactic coordinates ( $h_{75}^{-1} \text{ Mpc}$ ).

Column (7): Bahcall and Soneira (1984) catalog number.

Column (8): Batuski and Burns (1985a) catalog number ( $c = \text{core}$ ;  $n = \text{neighborhood}$ ).

TABLE 1  
 FIVE SUPERCLUSTER COMPLEXES

Name	z	SGX	SGY	SGZ	Bahcall & Soneira	Batuski & Burns
PISCES-CETUS SUPERCLUSTER COMPLEX						
Pisces-Cetus Supercluster						
Abell						
* 14	0.0640	3.	-229.	10.	...	5c, 3n
* 44	0.0559	119.	-161.	33.	...	...
* 74	0.0672	16.	-238.	-10.	...	5c, 3n
* 75	0.0617	158.	-152.	35.	...	5c
* 76	0.0416	82.	-131.	15.	...	5c
* 77	0.0719	203.	-145.	47.	...	5n
* 79	0.0927	214.	-228.	45.	...	1n
* 85	0.0518	54.	-182.	2.	1	5c, 56n
* 86	0.0610	18.	-218.	-11.	...	5c
* 104	0.0822	216.	-182.	38.	...	...
* 114	0.0566	19.	-203.	-19.	...	5c
* 117	0.0536	57.	-187.	-10.	...	56c, 5n, 55n
* 119	0.0440	70.	-147.	-2.	2	5c, 56n
* 133	0.0604	22.	-215.	-28.	...	5c
* 147	0.0438	80.	-141.	-7.	...	5c
* 150	0.0596	139.	-164.	1.	...	5c
* 151	0.0526	41.	-186.	-25.	1	5c, 56n
* 154	0.0658	165.	-167.	4.	3	5c
* 158	0.0645	160.	-166.	3.	...	5c
* 160	0.0447	112.	-122.	0.	...	5c
* 168	0.0452	78.	-147.	-14.	2	5c, 56n
* 171	0.0706	172.	-181.	-3.	...	5c
* 179	0.0547	146.	-136.	-3.	...	5c
* 189	0.0334	63.	-108.	-14.	2	5c, 7n
* 193	0.0482	106.	-141.	-15.	2	5c
* 195	0.0422	115.	-107.	-6.	...	5c
* 225	0.0692	181.	-165.	-21.	3	5c, 60n
* 240	0.0618	132.	-175.	-35.	...	5c
* 245	0.0790	160.	-219.	-48.	...	5c, 57n
* 246	0.0700	142.	-198.	-44.	...	5c, 57n
* 257	0.0947	171.	-178.	-38.	...	59c
* 277	0.0467	79.	-147.	-42.	...	...
* 279	0.0815	144.	-283.	-92.	...	57c
* 281	0.0880	122.	-233.	-71.	...	...
* 2665	0.0559	92.	-263.	-86.	...	5c, 57n
			-171.	60.	...	52c, 5n
Perseus-Pegasus Chain						
Abell						
* 71	0.0220	67.	-48.	17.	...	5c
* 262	0.0161	57.	-26.	-2.	...	8c
* 347	0.0187	69.	-21.	-7.	...	8c
* 426	0.0183	67.	-15.	-17.	...	8c
* 2506	0.0331	57.	-90.	66.	...	...
* 2572	0.0395	84.	-101.	68.	...	5c
Virgo-Hydra-Centaurus Supercluster						
Abell						
1060	0.0114	-27.	23.	-27.	...	...
non-Abell						
1228, 3+1240	0.0039	-4.	15.	-1.	...	...
1246, 0-4103	0.0107	-38.	16.	-8.	...	...
1346, 3-3012	0.0145	-49.	29.	3.	...	...
1400, 7-3344	0.0138	-48.	24.	5.	...	...
1611, 0-6045	0.0176	-67.	-10.	8.	...	...
1957, 2-3840	0.0186	-45.	-40.	40.	...	...
Sculptor Region						
Abell						
194	0.0178	31.	-61.	-9.	...	7c
260	0.0348	116.	-61.	-7.	...	58c
397	0.0325	89.	-69.	-49.	...	7c
400	0.0232	53.	-59.	-41.	...	7c
non-Abell						
0023, 0-3318	0.0497	-23.	-181.	-8.	...	...
0105, 1-4708	0.0230	-28.	-81.	-21.	...	...
0107, 6-4610	0.0240	-28.	-85.	-22.	...	...
0237, 5-3124	0.0210	-1.	-70.	-41.	...	...
0410, 6-6252	0.0170	-36.	-40.	-38.	...	...
0621, 6-6426	0.0265	-65.	-40.	-66.	...	...
2345, 0-2824	0.0279	-10.	-105.	13.	...	...
2349, 1-2839	0.0370	-13.	-138.	14.	...	...
2349, 3-3442	0.0310	-22.	-115.	7.	...	...
Pegasus-Pisces Chain						
Abell						
16	0.0838	144.	-245.	55.	...	...
2618	0.0705	161.	-161.	103.	...	52c, 99n
2622	0.0621	155.	-131.	93.	...	52c
2625	0.0609	136.	-148.	87.	...	52c
2626	0.0573	130.	-139.	83.	...	52c
2630	0.0675	135.	-176.	92.	...	52c, 99n
2675	0.0726	136.	-203.	76.	...	52c
2694	0.0958	163.	-268.	83.	...	53c
2700	0.0978	136.	-292.	74.	...	53c
non-Abell						
0008, 0+1056	0.0890	168.	-244.	72.	...	...

TABLE 1—Continued

Name	z	SGX	SGY	SGZ	Bahcall & Soneira	Batuzki & Burns
<b>AQUARIUS SUPERCLUSTER COMPLEX</b>						
<b>Aquarius-Capricornus Region</b>						
Abell						
2366	0.0542	3.	-145.	134.	...	50c, 51n
2377	0.0808	-8.	-214.	182.	...	51c, 50n, 93n
2382	0.0648	-23.	-185.	137.	...	50c, 94n
2384	0.0943	-51.	-261.	179.	...	94c, 48n, 50n
2388	0.0615	58.	-143.	158.	...	...
2399	0.0587	7.	-165.	134.	...	50c
2400	0.0881	-7.	-241.	183.	...	51c, 50n, 93n, 96n
2410	0.0806	2.	-224.	169.	...	51c, 50n, 96n
2412	0.0735	-42.	-219.	132.	...	50c, 94n
2415	0.0597	18.	-168.	133.	...	50c, 51n
2420	0.0838	-3.	-240.	163.	...	51c, 50n, 96n
2440	0.0904	56.	-245.	180.	...	50c
2448	0.0810	26.	-240.	146.	...	50c
2457	0.0597	54.	-171.	120.	...	50c
2459	0.0736	-3.	-231.	118.	...	50c, 51n, 100n
2462	0.0698	-8.	-223.	107.	...	50c, 100n
2469	0.0656	97.	-164.	136.	...	99n
<b>Aquarius Region</b>						
Abell						
* 2528	0.0955	-16.	-307.	101.	...	100c
* 2538	0.0817	-6.	-269.	89.	...	100c, 50n
* 2556	0.0865	-12.	-285.	85.	...	100c
* 2559	0.0796	24.	-260.	94.	...	50c, 100n
* 2566	0.0821	-5.	-273.	81.	...	100c
* 2597	0.0852	39.	-278.	89.	...	50c
* 2638	0.0825	47.	-273.	71.	...	50c
* 2670	0.0745	54.	-251.	52.	...	50c
<b>HERCULES-CORONA BOREALIS SUPERCLUSTER COMPLEX</b>						
Abell						
1691	0.0722	48.	244.	57.	...	38c
1749	0.0590	32.	202.	60.	...	38c
* 1775	0.0696	-13.	235.	73.	12a	38c
* 1781	0.0762	2.	254.	84.	...	38c
* 1793	0.0849	14.	276.	97.	12a	38c
* 1795	0.0616	-12.	209.	71.	12a	38c
* 1800	0.0724	-7.	241.	84.	...	38c
* 1813	0.0962	33.	303.	116.	...	38c
* 1825	0.0618	-35.	206.	75.	...	38c

TABLE 1—Continued

Name	z	SGX	SGY	SGZ	Bahcall & Soneira	Batuski & Burns	Name	z	SGX	SGY	SGZ	Bahcall & Soneira	Batuski & Burns
OUTSIDE FIVE MAJOR SUPERCLUSTER COMPLEXES													
Abell													
21	0.0948	247.	-189.	82.	...	2n	680	0.0790	149.	179.	-148.	...	23c, 69n
102	0.0657	108.	-208.	8.	...	5c, 56n	690	0.0788	119.	178.	-172.	...	68c
116	0.0669	109.	-212.	-0.	...	5c, 56n	695	0.0687	116.	161.	-142.	...	23c
134	0.0694	102.	-224.	-11.	...	56c, 5n	779	0.0226	37.	66.	-43.	...	73c
272	0.0877	268.	-136.	-17.	...	9c, 58n	991	0.0989	122.	285.	-122.	...	...
278	0.0896	269.	-145.	-23.	...	9c, 58n	1035	0.0792	107.	245.	-70.	6	27c, 73n
358	0.0576	62.	-177.	-92.	...	10c	1097	0.0793	65.	257.	-80.	...	27c, 31n
376	0.0489	166.	-60.	-35.	...	12c	1126	0.0852	-1.	271.	-113.	...	25n
399	0.0715	174.	-150.	-106.	...	14c	1187	0.0791	89.	258.	-42.	6	27c, 26n, 73n
401	0.0748	183.	-154.	-110.	4	14c	1365	0.0763	38.	263.	-30.	...	27c, 26n, 34n, 73n
404	0.0632	215.	-55.	-45.	4	12c	1399	0.0913	-127.	271.	-87.	9	27c, 26n
407	0.0470	159.	-55.	-44.	...	12c	1609	0.0891	-2.	304.	27.	...	75c
410	0.0897	173.	-204.	-152.	...	...	1630	0.0649	-86.	215.	2.	...	...
415	0.0788	87.	-209.	-156.	...	...	1631	0.0508	-122.	139.	-15.	...	37c
419	0.0406	18.	-121.	-90.	...	15c	1644	0.0449	-114.	120.	-12.	...	37c
423	0.0797	87.	-208.	-162.	...	15c	1650	0.0845	-139.	257.	2.	...	...
449	0.0803	268.	-76.	26.	...	62n	1651	0.0825	-147.	246.	-0.	...	...
450	0.0607	174.	-81.	-105.	...	...	1736	0.0360	-108.	76.	-1.	...	37c
465	0.0855	171.	-150.	-187.	...	16c	1750	0.0860	-150.	252.	42.	...	39c
478	0.0900	192.	-124.	-207.	...	16c	1773	0.0776	-123.	235.	56.	11	39c
480	0.0473	85.	-83.	-128.	...	...	1809	0.0788	-114.	240.	73.	11	39c
484	0.0386	51.	-77.	-111.	...	...	1836	0.0363	-90.	98.	29.	...	...
496	0.0320	30.	-61.	-100.	...	...	1837	0.0376	-92.	102.	31.	...	...
500	0.0666	22.	-127.	-200.	...	...	2028	0.0772	-105.	197.	152.	14	43c, 38n
505	0.0543	182.	73.	24.	5	18c	2029	0.0767	-112.	192.	151.	14	43c, 38n
509	0.0836	137.	-102.	-233.	...	62c	2033	0.0821	-116.	204.	161.	...	38c, 43n
514	0.0731	29.	-128.	-222.	...	18c	2048	0.0945	-140.	223.	184.	14	43n
526	0.0541	100.	-56.	-160.	...	...	2168	0.0619	94.	141.	144.	...	44n, 85n, 88n
533	0.0472	11.	-80.	-154.	...	62c	2184	0.0550	73.	125.	138.	...	85n
539	0.0205	40.	-17.	-66.	...	18c	2198	0.0798	74.	171.	207.	...	45c, 46n
548	0.0410	-7.	-49.	-145.	...	...	2247	0.0392	115.	70.	57.	...	89c
553	0.0670	205.	70.	-101.	...	...	2248	0.0663	176.	117.	107.	...	89c
559	0.0757	240.	113.	-21.	...	62c, 20n	2250	0.0654	54.	115.	196.	...	45c, 46n
564	0.0779	242.	123.	-21.	...	20c, 19n, 62n	2255	0.0800	166.	141.	173.	...	...
566	0.0984	289.	151.	-63.	...	20c, 19n	2256	0.0601	165.	104.	94.	...	89c
568	0.0751	177.	102.	-167.	...	64n	2271	0.0568	156.	98.	92.	...	89c
569	0.0196	60.	33.	-33.	...	21c	2295	0.0508	127.	81.	109.	...	89c
576	0.0381	117.	69.	-45.	...	21n	2296	0.0617	170.	99.	102.	...	89c
582	0.0581	148.	99.	-111.	...	64c, 22n	2301	0.0874	210.	125.	175.	...	47c, 89n
592	0.0624	63.	83.	-198.	...	...	2319	0.0564	94.	29.	179.	...	...
595	0.0666	181.	128.	-86.	...	...	non-Abell					...	
623	0.0871	24.	114.	-276.	...	...	0022.2-5712	0.0450	-83.	-142.	-26.	...	...
628	0.0835	164.	167.	-170.	...	...	0035.0-0126	0.0735	106.	-236.	18.	...	...
634	0.0267	79.	60.	-26.	...	23c	0258.3-3714	0.0360	-16.	-111.	-76.	...	...
644	0.0704	-11.	92.	-232.	...	21c	0317.9-5403	0.0550	-80.	-146.	-111.	...	...
671	0.0494	86.	112.	-113.	...	23n	0329.2-5247	0.0569	-79.	-148.	-120.	...	...
					...	...	0341.9-5349	0.0575	-84.	-144.	-125.	...	...

TABLE 1—Continued

Name	z	SGX	SGY	SGZ	Bahcall & Soneira	Batuski & Burns	Name	z	SGX	SGY	SGZ	Bahcall & Soneira	Batuski & Burns	
<b>LEO SUPERCLUSTER COMPLEX</b>														
<b>Near Leo Region</b>														
Abell														
* 754	0.0528	-36.	99.	-161.	...	25c	1362	0.0966	-77.	306.	-84.	...	25c, 35n	
* 780	0.0545	-49.	103.	-163.	...	25c	* 1371	0.0673	-26.	233.	-49.	...	35c, 25n	
* 838	0.0502	-33.	117.	-139.	...	25c	* 1385	0.0831	-51.	276.	-63.	...	...	
* 957	0.0440	-32.	123.	-102.	...	25c	* 1390	0.0796	-47.	267.	-58.	...	25c, 35n	
* 978	0.0527	-57.	139.	-121.	...	25c	* 1474	0.0791	-42.	271.	-33.	...	25c, 35n, 36n, 77n	
* 979	0.0550	-63.	142.	-127.	...	25c	* 1526	0.0797	-53.	272.	-19.	...	77c, 25n, 36n	
* 992	0.0533	22.	171.	-90.	...	25c	* 1541	0.0892	-85.	293.	-22.	...	35n, 77n	
* 993	0.0533	-53.	143.	-120.	...	...	* 1552	0.0845	-68.	284.	-14.	...	77c, 25n, 36n	
* 999	0.0318	-1.	103.	-62.	...	...	* 1569	0.0784	-44.	270.	1.	...	36c, 25n, 77n	
* 1016	0.0321	-5.	104.	-63.	...	...	* 1589	0.0718	-34.	251.	8.	...	36c	
* 1069	0.0630	-82.	167.	-129.	...	25c	* 1638	0.0621	-31.	220.	19.	...	36c	
* 1100	0.0464	16.	159.	-62.	...	25c	<b>URSA MAJOR SUPERCLUSTER COMPLEX</b>							...
* 1139	0.0386	-36.	123.	-67.	...	25c	Abell							...
* 1142	0.0353	-15.	121.	-53.	...	25c	757	0.0517	114.	137.	-63.	...	...	
* 1177	0.0316	6.	114.	-36.	...	25c	834	0.0707	187.	166.	-9.	...	67c	
* 1185	0.0304	18.	111.	-28.	7	25c, 31n	* 945	0.0917	231.	211.	10.	...	67c, 74n	
* 1213	0.0468	27.	166.	-38.	...	25c, 31n	* 1003	0.0520	95.	160.	-37.	...	26c	
* 1216	0.0524	-71.	159.	-80.	...	25c, 32n	* 1169	0.0582	82.	192.	-26.	...	26c, 27n	
* 1228	0.0350	30.	127.	-22.	7	31c, 25n, 26n, 27n, 29n	* 1186	0.0791	209.	175.	44.	...	30c, 67n	
* 1257	0.0339	30.	123.	-18.	...	32c, 25n	* 1218	0.0792	134.	241.	-9.	...	33c, 34n	
* 1267	0.0321	12.	118.	-24.	...	29c, 26n, 31n	* 1254	0.0628	160.	155.	31.	...	30n, 67n	
* 1308	0.0481	-69.	150.	-63.	...	31c, 25n, 26n, 27n, 29n	* 1270	0.0689	124.	211.	3.	...	33c	
* 1314	0.0341	55.	116.	-2.	...	32c, 25n	* 1279	0.0603	55.	209.	-26.	...	26c, 27n, 29n, 31n	
* 1334	0.0559	-83.	173.	-68.	...	29c	* 1291	0.0551	134.	147.	23.	...	67c	
* 1367	0.0215	-3.	81.	-15.	10	32c, 25n	* 1318	0.0530	102.	164.	7.	8	33c	
* 1656	0.0232	1.	88.	13.	10	32c, 25n	* 1377	0.0566	105.	176.	7.	8	33c	
<b>Far Leo Region</b>														
Abell														
744	0.0729	54.	177.	-179.	...	70n	* 1400	0.0778	136.	235.	19.	...	33c	
763	0.0840	55.	203.	-200.	...	70c	* 1412	0.0839	209.	193.	55.	...	30c, 67n	
819	0.0759	14.	192.	-183.	...	...	* 1436	0.0646	117.	198.	23.	...	33c	
858	0.0881	-9.	221.	-207.	...	...	* 1452	0.0631	100.	202.	18.	...	33c, 26n	
912	0.0888	-48.	223.	-202.	...	71n	* 1461	0.0537	59.	187.	6.	...	26c, 33n	
933	0.0958	-53.	244.	-208.	...	72c, 25n	* 1468	0.0844	127.	262.	24.	...	33c, 76n	
954	0.0922	-58.	239.	-196.	...	72n	* 1496	0.0941	172.	265.	46.	...	67c	
1020	0.0650	-12.	198.	-120.	...	25c	* 1500	0.0720	184.	167.	54.	...	67c, 30n	
1032	0.0794	-43.	227.	-152.	...	72c, 25n	* 1507	0.0592	117.	176.	33.	...	33c	
1145	0.0677	-4.	225.	-87.	...	25c	* 1534	0.0698	139.	200.	44.	...	...	
1149	0.0710	-41.	225.	-104.	...	25c	* 1616	0.0833	131.	250.	59.	...	33c	
1171	0.0704	-61.	218.	-105.	...	25c	* 1681	0.0908	210.	213.	84.	...	...	
1238	0.0716	-76.	222.	-94.	...	25c	* 1741	0.0745	175.	179.	77.	...	...	
* 1337	0.0826	-53.	271.	-74.	...	25c, 32n	* 1767	0.0701	123.	201.	79.	...	33c, 67n	
1346	0.0970	-85.	304.	-91.	...	...	* 1783	0.0766	117.	224.	90.	...	33n	
* 1356	0.0698	-46.	235.	-61.	...	35c, 25n	* 1851	0.0864	199.	197.	101.	...	...	
					...	...	1904	0.0988	166.	260.	126.	...	...	
					...	...	non-Abell	0.0708	78.	211.	110.	...	...	
					...	...	* 1101.0+7042	0.0843	209.	201.	31.	...	...	

TABLE 1—Continued

Name	z	SGX	SGY	SGZ	Bahcall & Soneira	Batuski & Burns	Name	z	SGX	SGY	SGZ	Bahcall & Soneira	Batuski & Burns
0427.8-5350	0.0384	-61.	-87.	-97.	...	...	† 2131.0-5351	0.0772	-171.	-200.	60.	...	...
0430.5-6135	0.0545	-107.	-115.	-121.	...	...	† 2137.0-2245	0.0331	-28.	-99.	71.	...	...
0600.2-4002	0.0490	-53.	-62.	-160.	...	...	† 2142.1-5150	0.0535	-117.	-150.	45.	...	...
0608.5-3335	0.0350	-27.	-37.	-123.	...	...	† 2143.1-5732	0.0743	-172.	-193.	40.	...	...
0626.5-5422	0.0502	-98.	-63.	-143.	...	...	† 2147.0-5533	0.0675	-152.	-181.	42.	...	...
0820.0+0647	0.0809	44.	139.	-241.	...	...	† 2150.6-5805	0.0760	-174.	-198.	36.	...	...
0820.0+0647	0.0809	44.	139.	-241.	...	...	† 2152.3-5549	0.0376	-89.	-107.	23.	...	...
0935.6-2007	0.0335	-51.	61.	-98.	...	...	† 2156.5-5624	0.0754	-167.	-202.	39.	...	...
1251.6-2845	0.0553	-162.	116.	-27.	...	...	† 2158.2-6011	0.0996	-224.	-248.	33.	...	...
1326.0-3100	0.0479	-151.	92.	-3.	...	...	† 2201.1-5822	0.0405	-97.	-114.	17.	...	...
1843.0+4530	0.0918	135.	79.	271.	...	...	† 2201.2-5019	0.0365	-76.	-110.	29.	...	...
† 2006.0-5639	0.0585	-162.	-123.	59.	...	...	† 2212.7-5148	0.0680	-135.	-196.	41.	...	...
† 2029.1-6312	0.0763	-210.	-161.	42.	...	...	† 2213.5-5250	0.0532	-110.	-157.	31.	...	...
† 2035.9-6132	0.0709	-192.	-155.	44.	...	...	† 2218.2-5523	0.0396	-88.	-118.	18.	...	...
† 2047.8-5255	0.0446	-113.	-110.	49.	...	...	† 2221.0-5644	0.0590	-129.	-168.	21.	...	...
† 2048.7-5208	0.0467	-116.	-116.	53.	...	...	† 2222.4-5605	0.0789	-164.	-219.	29.	...	...
† 2059.0-2813	0.0379	-54.	-101.	85.	...	...	† 2228.5-5500	0.0752	-152.	-214.	28.	...	...
† 2104.0-3955	0.0520	-99.	-138.	85.	...	...	† 2231.8-5243	0.0554	-110.	-167.	25.	...	...
† 2104.3-2541	0.0385	-48.	-103.	88.	...	...	2244.0+3925	0.0820	211.	-102.	161.	...	...
† 2113.1-5937	0.0588	-151.	-145.	35.	...	...	2339.0+2632	0.0952	226.	-193.	127.	...	...
† 2126.1-5102	0.0797	-170.	-207.	74.	...	...	2336.0-6112	0.0959	-186.	-264.	-40.	...	...
† 2130.7-6215	0.0555	-144.	-139.	22.	...	...						...	...

## REFERENCES

- Bahcall, N. A., and Soneira, R. M. 1983, *Ap. J.*, **270**, 20.  
 ———. 1984, *Ap. J.*, **277**, 27.  
 Batuski, D. J., and Burns, J. O. 1985a, *A.J.*, **90**, 1413.  
 ———. 1985b, *Ap. J.*, **299**, 5.  
 Batuski, D. J., Melott, A., and Burns, J. O. 1987, in *IAU Symposium 124, Observational Cosmology*, ed. G. R. Burbidge, A. Hewitt, and L. Z. Fang (Dordrecht: Reidel) p. 323.  
 Ciardullo, R., Ford, H., Bartko, F., and Harms, R. 1983, *Ap. J.*, **273**, 24.  
 Ciardullo, R., Ford, H., and Harms, R. 1985, *Ap. J.*, **293**, 69.  
 Corwin, H. G., Jr., and Emerson, D. 1982, *M.N.R.A.S.*, **200**, 621.  
 Einasto, J., Klypin, A. A., Saar, E., and Shandarin, S. F. 1984, *M.N.R.A.S.*, **206**, 529.  
 Henry, J. P., and Huchra, J. P. 1987, private communication.  
 Huchra, J. P., and Postman, M. 1986, private communication.  
 Postman, M., Geller, M. J., and Huchra, J. P. 1986, *A.J.*, **91**, 1267.  
 Shectman, S. A. 1985, *Ap. J. Suppl.*, **57**, 77.  
 Struble, M. F., and Rood, H. J. 1987, *Ap. J. Suppl.*, **63**, 543.  
 Tully, R. B. 1986, *Ap. J.*, **303**, 25 (T86).  
 ———. 1987, *Nearby Galaxies Catalog* (Cambridge: Cambridge University Press) (NBG catalog).  
 Tully, R. B., and Fisher, J. R. 1987, *Nearby Galaxies Atlas* (Cambridge: Cambridge University Press).

R. BRENT TULLY: Institute for Astronomy, 2680 Woodlawn Drive, Honolulu, Hawaii